Enhanced Blue Emission from Transparent Oxyfluoride Glass Ceramics Containing Pr^{3+}:BaF_2 Nano-crystals

Kaushik Biswas[†], Atul D. Sontakke[†], Jiten Ghosh[‡] and Kalyandurg Annapurna[†,*]

[†]Glass Technology Laboratory, [‡]X-ray diffraction Section
Central Glass and Ceramic Research institute, CSIR
196, Raja S. C. Mullick Road, Kolkata – 700 032, India

Abstract

Transparent glass ceramics containing Pr^{3+}:BaF_2 nano-crystals in chemical composition of SiO_2–BaF_2–K_2CO_3–La_2O_3-Sb_2O_3 oxyfluoride glass systems have been prepared from melt quenching and with subsequent heat-treatment method. Luminescence and structural properties of these materials have been evaluated and the results are reported. Rietveld analysis of X-ray diffraction (XRD) patterns and investigation of transmission electron microscopy (TEM) confirmed the presence of BaF_2 nano-crystals dispersed in the heat treated glass matrices. Measured UV-Vis-NIR absorption spectra have exhibited nine bands of the transitions $^3H_4 \rightarrow {}^3P_2$, ($^1I_6$, $^3P_1$), $^3P_0$, $^1D_2$, $^1G_4$, $^3F_3$,$^3F_2$, $^3H_6$ and $^3H_5$ from all the samples with non-degenerated $^1I_6$ and $^3P_1$ levels in the glass ceramics. The photoluminescence spectra show an enhancement in the intensities upon ceramization indicating the incorporation of Pr^{3+} ions in BaF_2 nano-crystals which possess low phonon energy (346 cm^{-1}). This has further been corroborated from the observation of a significant 3-fold increase in the relative intensity ratio of blue ($^3P_0 \rightarrow {}^3H_4$) to red ($^1D_2 \rightarrow {}^3H_4$, $^3P_0 \rightarrow {}^3H_6$) emissions from glass-ceramics compared with the glass. It is due to a significant decrease of multiphonon non-radiative relaxation from $^3P_0$ to $^1D_2$ level of Pr^{3+} in glass ceramics. Time resolved spectra exhibit $^3P_0$ level decays faster than $^1D_2$ level.

Keywords : Oxyfluoride transparent glass-ceramics; Pr^{3+}:BaF_2 nano-crystals; luminescence

Supported by Mega Laboratory Project–MLP0101

[*] Author to whom correspondence should be addressed. e-mail: annapurnak@cgcri.res.in

I. Introduction

Rare earth doped transparent host materials have been widely investigated over the past decades due to the increasing demand of high quality optical devices for telecommunication systems such as fibre, optical amplifiers and solid state lasers.[1-2] Recently, oxyfluoride glass ceramic system has been considered as a more promising host material for several active optical applications because of the fact that it combines both low phonon energy due to fluorides environment, and high chemical durability with superior mechanical stability in an oxide environment.[3-6] When the rare earth ions are incorporated into low phonon energy sites of fluoride nano-crystallites (300-400 cm^{-1}), they exhibit efficient fluorescent properties with an enhanced emission efficiency and longer lifetimes because of the reduced non-radiative relaxations. Furthermore, these glasses exhibit superior thermal stability and fiberizability than the fluoride-based glasses. Thus, rare earth doped oxyfluoride glass ceramics are considered to be suitable materials for low-loss, high strength low-cost optical fibres, laser active media and up-conversion solar cell applications.

Most of the investigations on rare earth doped transparent oxyfluoride glass ceramics have been focussed on oxide glass matrix containing PbF_2, CdF_2, LaF_3 crystals.[4,7-12] But, these glasses were usually synthesized from toxic heavy metal fluorides such as CdF_2 and PbF_2. Recently, significant attention was devoted on the synthesis of transparent oxyfluoride glass ceramics having alkaline-earth fluoride crystals like Ba, Ca, and Sr as these crystals have high solubility of both sensitizer and activator rare earth ions.[13] Among the alkaline earth fluorides, rare earth doped BaF_2 single crystal has been found to be an attractive host material for laser and up-conversion devices due to its low phonon energy and large energy transfer coefficient between the rare earth ions.[14] Some preliminary investigations on the optical and

photoluminescence properties on oxyfluoride glass ceramics having BaF_2 nano-crystals have been reported.[15,16]

In RE ion family, Pr^{3+} is an attractive optical activator because of its unique energy-level structure. It offers the possibility of simultaneous blue and red emissions in visible for laser action and NIR emission at 1.3 μm for optical amplification.[17] Further, trivalent praseodymium has been well known active ion exhibiting quantum cutting (QC) or up-conversion emission either by singly or co-doped with other rare earth ions. There are few studies on the luminescence of Pr^{3+} in low phonon energy BaF_2 single crystals.[18,19] However, Pr^{3+} doped BaF_2 nano-crystals containing transparent oxyfluoride glass ceramics have not been explored.

Thus, in the present work, Pr^{3+} doped oxyfluoride glass system was undertaken which yields BaF_2 nano-crystalline-glass composite on ceramization. For this study, the base glass composition having a good thermal stability was selected from the work of Yu et. al.[15] The effect of ceramization on the structural, optical and photoluminescence properties of this oxyfluoride glass system has been studied from the measurement of DTA, XRD, TEM, FTIR, optical absorption, excitation and emission spectra.

II. Experimental procedure

(1) Sample preparation

Pr^{3+} doped oxyfluoride glasses in the composition of (mol %) $67.7SiO_2$–$14.9BaF_2$–$12.9K_2CO_3$–$3La_2O_3$-$1.0Sb_2O_3$-$0.5Pr_2O_3$ were prepared by quenching method. The glasses were synthesized using high purity raw materials such as SiO_2 (99.8%, Sipur A1 Bremtheler Quartzitwerk, Usingen, Germany), BaF_2 (99.99 %, Merck KgaA, Darmstadt, Germany),

K_2CO_3 (99.9 %, Loba Chemie Pvt. Ltd., Mumbai, India), La_2O_3 (99.9 % Alfa Aesar, Ward Hill, MA), Sb_2O_3 (99.9 %, Merck KgaA, Darmstadt, Germany) and Pr_6O_{11} (99.9%, Alfa Aesar**,** Karlsruhe, Germany). The well mixed chemical batches of about 30 g glasses were melted in covered platinum crucible in air at 1400^{o}C for 1 h. The melt was homogenized with an intermittent stirring at regular intervals and then cast onto a graphite mould. The cast samples were annealed at 450^{o}C for 1 h followed by controlled cooling to room temperature in order to release the internal stresses. To prepare the glass ceramics, the glass samples were heat-treated at 600^{o}C for 4 h and 24 h. The resulted glass and glass ceramic samples were labelled as "OFPrG", "OFPrGC04" and "OFPrGC24" respectively. These samples were cut to the desired sizes and processed for carrying out further characterization experiments.

(2) Characterization techniques

Refractive indices of glass and glass ceramic samples were measured at five wavelengths (473 nm, 532 nm, 633 nm, 1064 nm, and 1552 nm) on a Prism Coupler (Metricon Model-2010, NJ, USA) fitted with five different lasers as illuminating sources. The densities (*d*) of glass and glass ceramic samples were measured by following Archimedes' principle using water as buoyancy liquid on Mettler Tollado balance fitted with density measurement kit. The differential thermal analysis (DTA) of the glass was performed in the temperature range of room temperature to 700^{0}C on a differential thermal analyzer (model STA 409, Netzsch-Gerätebau GmbH, Selb, Germany) at a heating rate of 20 K/min to obtain various thermal data.

The X-ray diffraction (XRD) patterns of the glass and glass ceramic samples were recorded using an X'pert Pro MPD diffractometer (PANalytical, Almelo, The Netherlands) using X'Celerator operating at 40kV and 30 mA using Ni-filtered CuK_α radiation with wavelength

of 1.5418367 Å. The XRD data were recorded in step-scan mode with step size 0.05^0 (2θ) and step time 15 sec from 10^0 to 80^0. Weight percentages of crystalline and amorphous phases were estimated for these samples from XRD line profile analysis using Rietveld method[20,21] by X'pert high score plus software (PANalytical).[22] Rietveld method is a full-pattern fit method. This is basically a non-linear least square method. The measured profile and the calculated profile are compared. By the variation of many parameters the least squares refinements are carried out until the residuals are minimized and best fit is achieved between the entire observed powder diffraction pattern taken as a whole and the entire calculated pattern based on simultaneously refined models for crystal structures, instrumental factors, diffraction optics effects and other specimen characteristics (lattice parameters, size and strain parameters). Wt.% of amorphous BaF_2 phase has been estimated for experimental samples from XRD line profile analysis using Rietveld analysis by X'Pert high score plus software (PANalytical). Only crystalline phases are taken into account and their sum is normalized to 100% during the Rietveld refinement. The amount of the crystalline phases is overestimated in case amorphous material is present too. This effect can actually used to estimate the amorphous content in the material.[23] An internal standard (a known amount of a pure crystalline phase) added with the sample to estimate the amorphous content from the overestimation of this phase (and all other phases) from XRD analysis by X'Pert high score plus software (PANalytical).

The microstructure of the glass ceramic samples was investigated by transmission electron microscope (TEM) (FEI Model Tecnai G2 30ST, Hillsboro, OR, USA). Samples for TEM measurement were prepared by dispersing finely powdered sample in ethanol, followed by an ultrasonic agitation, and then its deposition onto the carbon-enhanced copper grid. The FTIR reflectance spectra of all Pr^{3+}-doped glass and glass ceramic samples were recorded using a FTIR spectrometer (Model 1615, Perkin–Elmer, Norwalk, CT) in the wavenumber range of

400–1500 cm^{-1} at a 15^{o} angle of incidence. The optical absorption spectra were recorded on a Perkin Elmer UV–Vis spectrophotometer (Model Lambda 20, Perkin Elmer, Waltham, MA, USA) in the wavelength range 300–1100 nm. The NIR absorption spectra of all Pr^{3+}-doped glass and glass ceramic samples were recorded using a FT-IR spectrometer (Model Spectrum 100, Perkin Elmer, Waltham, MA, USA) in the wavenumber range of 400-7800 cm^{-1}.

The steady state PL spectra were measured on a SPEX spectrofluorimeter (Model Fluorolog-II, SPEX CertiPrep, Metuchen, NJ, USA) using 150 W continuous Xe lamp as the excitation source and the time resolved fluorescence spectra and emission decay kinetics were measured on the same instrument equipped with 1934D phosphorimeter attachment by using 50 W pulsed xenon lamp as the pump source. The system employs Datamax software in acquiring the spectral data and the decay curves.

III. Results and discussion

(1) Physical and optical properties

The glass precursor and glass ceramic samples are both transparent as shown in Fig. 1. All these samples are in green colour arising from the presence and uniform distribution of Pr^{3+} ions. The measured refractive indices of all samples at five different wavelengths are listed in Table I which have been used to obtain refractive indices ($n_{F'}$, n_e, $n_{C'}$) at standard wavelengths $\lambda_{F'}$ = 480 nm, λ_e = 546.1 nm and $\lambda_{C'}$ = 643.8 nm respectively from Cauchy dispersion fitting. Other physical and optical properties estimated using standard expressions from the measured density (d) and refractive indices ($n_{F'}$, n_e, $n_{C'}$) are also presented in Table I. From this data, it can be observed that upon ceramization, the density and refractive indices of the glass ceramic samples decrease. The decrease in density can be attributed to an

increase in the number of non-bridging oxygen in the residual glass matrix upon ceramization of BaF_2 nano-crystals followed by an expansion of overall glass network. Similar observation was also found by Bocker et al.[24] where it was observed that the density of glass ceramics samples decreased with an increase in the crystalline volume fraction of BaF_2 in glass matrix. Similarly, the decrease in refractive indices with ceramization is due to the fact that BaF_2 has a lower refractive index (1.4733 at 632.8 nm) compared to the precursor glass (1.5476 at 632.8 nm). All other related properties listed in Table I vary according to the changes observed in refractive indices and densities of glass and glass-ceramic samples.

(2) Thermal and structural analysis

Fig. 2 depicts the DTA thermogram of powdered OFPrG sample which shows an endothermic peak corresponding to glass transition event followed by an exothermic peak related to crystallization event. The glass transition temperature (T_g), the crystallization onset temperature (T_x), and crystallization peak temperature (T_p) were estimated to be 513^{o}C, 580^{o}C and 600^{o}C respectively. From this data, the glass forming ability (GFA) determined by glass stability factor ($\Delta T = [T_x - T_g]$) has been found to be 67^{o}C indicating the good stability of the glass which can undergo a controlled crystallization to yield nano-crystalline glass ceramic composite.

The X-ray diffraction pattern of the as-quenched glass (OFPrG) in Fig. 3 consists of broad halos confirming its amorphous nature. However, XRD patterns of the optimally ceramized OFPrGC04 and OFPrGC24 samples show distinct diffraction peaks which are in good agreement with face centred cubic (fcc) Barium Fluoride (BaF_2) crystal having space group *Fm -3m* (ICSD code: **041649**) and are indexed accordingly. The wt. % of crystalline and amorphous phases has been derived from Rietveld analysis and the data are summarized in Table II. The data show that there is a small increase in the phase fraction of BaF_2 with the

increase in duration of ceramization. This table also lists the values of average crystallite size and average lattice microstrain estimated from Rietveld analysis. The evaluated results of average crystallite size for the OFPrGC04 and OFPrGC24 samples are 7.86 nm and 7.70 nm signifying that the crystallite size remains almost unchanged with the increase in duration of ceramization time from 4 h to 24 h. Furthermore, it can be found in Table II that the lattice constant of ceramized samples decreased (0.617 nm) when compared to the lattice constant of BaF_2 bulk single crystal (0.620 nm). The lattice contraction during ceramization is due to the substitution of Ba^{2+} (ionic radius 0.142 nm) by Pr^{3+} (ionic radius 0.101 nm) in BaF_2 lattice. The quality of fitting was assessed from various numerical criteria of fit, namely the profile residual factor (R_p), the weighted residual factor (R_{wp}), the expected residual factor (R_{exp}), weighted- statistics (D_{ws}) and the goodness of fit (GOF) which reveal the good quality of the fitting. These reliability parameters of the fitting during Rietveld refinement are given in the Table III. The quality of the fittings of observed diffraction patterns with the simulated patterns are also shown by residual plots in Fig. 4 for OFPrGC24 sample.

The bright-field TEM image of OFPrGC04 sample in Fig. 5 (a) shows spherical crystallites (in dark appearance) sized 6-10 nm distributed homogeneously in a glass matrix. Fig. 5 (b) is the selected area electron diffraction (SAED) pattern displaying bright concentric rings occurring from the diffraction planes of polycrystalline phase. The indexing of diffraction ring pattern has been performed from their respective radii, which match with (111), (200) and (220) planes of face centred cubic BaF_2. It was examined from the TEM micrographs of OFPrGC24 sample (not shown in the figure) that the crystallite size remains almost unchanged when the ceramization time was increased to 24 h which is consistent with the XRD results as described above. Due to the smaller size of the precipitated BaF_2 nano-

crystals in comparison to the visible-near infrared wavelength, both the glass ceramic samples have sustained an excellent transparency.

Fig. 6 represents the recorded FTIR reflectance spectra of the glass and glass ceramic samples. For the OFPrG sample, intense reflection bands are located at 1039 cm^{-1}, 757 cm^{-1} and 459 cm^{-1}. These are attributed to asymmetric stretching vibration modes of Si–O bond involving bridging oxygen, symmetric stretching mode with inter-tetrahedral vibrations of [Si-O-Si] units and rocking vibration of oxygen atoms that move approximately perpendicular to the Si-O-Si planes (marked as $[Si\text{-}O\text{-}Si]_{As,}$ $[Si\text{-}O\text{-}Si]_{SS}$ and $[Si\text{-}O\text{-}Si]_{R}$ in the figure) respectively.[25] The vibrational bands in the 400–550 cm^{-1} region for all the samples are due to bending vibration of Si–O–Si linkage[26]. This spectral region may also overlap the specific vibrations of Ba-O bonds.[27] In the case of ceramized samples (OFPrGC04 and OFPrGC24), it is clearly seen from the figure that the band related to asymmetric stretching vibration mode of $[Si\text{-}O\text{-}Si]_{As}$ shifts towards a lower energy from 1039 cm^{-1} to 1021 cm^{-1} when compared to glass. More interestingly, in the ceramized samples, a well resolved reflection band is observed at 934 cm^{-1} corresponding to asymmetric stretching vibrations of Si–O bond involving non-bridging oxygen atoms (marked as $[Si\text{-}O^{-}]_{As}$ in the figure) of SiO_4 tetrahedra. The reason for its appearance could be due to the formation of nano-crystalline BaF_2 in the glass matrix, which makes the residual glass composition Ba-deficient in glass ceramics compared to the precursor glass composition. Thus, the formation of nano-crystalline BaF_2 in the glass matrix is responsible for the formation of non-bridging oxygen atoms in the residual glass matrix. Furthermore, the formation of Si-O-K becomes more probable than Si-O-Ba due to the depletion of Ba atoms in the residual glass network. As Ba atoms are introduced in the nano-crystalline BaF_2 structure, the peak corresponding to asymmetric stretching vibration mode of $[Si\text{-}O\text{-}Si]_{As}$ shifts to 1021 cm^{-1} from 1039 cm^{-1} as Si-

O-K linkage is weaker than Si-O-Ba linkage. However, the recorded FTIRRS epitomise mainly the silicate network in precursor and ceramized samples as the vibrational modes concerning the Ba–F bond of BaF_2 crystallites that occur below 400 cm^{-1} could not be detected because of the spectral range limitation of the instrument.[16]

(3) Absorption and emission spectral analysis

(A) UV-Vis-NIR absorption spectra:

Figs. 7 (a) and (b) show typical room temperature UV-Vis and NIR absorption spectra of all Pr^{3+}-doped glass and glass ceramic samples, respectively. Both spectra consist of absorption bands corresponding to the transitions between the ground state energy level $^3H_4$ and different excited states belonging to the $4f^2$ configuration of the trivalent praseodymium ions. From Fig 7 (a), it is observed that the transitions $^3H_4 \rightarrow {}^3P_2$, ($^1I_6$, $^3P_1$), $^3P_0$, $^1D_2$, and $^1G_4$ manifolds are centred at 444 nm, 469 nm, 480 nm, 590 nm and 994 nm respectively in case of OFPrG sample. The assignments of transitions have been made according to the energy level positions reported earlier for Pr^{3+} doped glasses. Among these transitions, $^3H_4 \rightarrow 3P_{0,\,1,\,2}$ complex group of Pr^{3+} ion could be mainly responsible for the green color of the samples.[28] The absorption peak at 469 nm corresponding to $^1I_6$ and $^3P_1$ is degenerated in the OFPrG sample because of the site to site disorder which usually exists in glassy phase. Similar such trends have previously been observed for many other Pr^{3+} doped glasses.[17] The inset of Fig. 7 (a) clearly shows that unlike in OFPrG sample, the peaks related to the transitions, $^3H_4 \rightarrow {}^1I_6$ and $^3P_1$ are non-degenerated in ceramized samples as two different bands at 464 nm and 470 nm confirming the incorporation of Pr^{3+} ions in the BaF_2 crystalline phase formed.

Another interesting observation related to the shape of the $^3H_4 \rightarrow {}^3P_0$ absorption band can be made from Fig. 7a. As such, with J = 0 of terminal level, this band is not expected to

display Stark splitting due to any crystal field effect similar to the peaks for $^7F_0 \rightarrow {}^5D_0$ of Eu^{3+} or $^4I_{9/2} \rightarrow {}^2P_{1/2}$ of Nd^{3+} ions. Hence the splitting of $^3H_4 \rightarrow {}^3P_0$ band of Pr^{3+} indicates the existence of non-equivalent sites for the dopant ion in that host matrix. In the present study, it is clearly evidenced that, this band exhibits multi peaks whose relative intensities are changing with glass to glass ceramic host. In case of OFPrG sample, the band has a maximum peak wavelength at 480 nm with a small sub peak at 477 nm, while in glass ceramic samples (OFPrGC4 and OFPrGC24), the peak at 477 nm has become more intense than the peak at 480 nm. This can be attributed due to the fact that, in oxyfluoride glass host, rare earth (Pr^{3+}) metal ion may have two coordination environments: one site may have only oxygen ligands (O-RE-O) and the other site may have oxy-fluoro/fluoro-fluoro ligands (O-RE-F/F-RE-F). The peak at 480 nm could be assigned to oxygen-coordinated site while the peak at 477 nm could be attributed to oxy-fluoro coordinated site. In glass, the O-RE-O site is more probable than other site and hence the corresponding peak is intense. But in glass ceramic samples, on incorporation of Pr^{3+} into BaF_2 crystalline phase, the second site apparently becomes dominant over the other which has been replicated in the recorded absorption spectra. Further, the UV absorption edge is shifted in the direction of longer wavelengths with the increase in degree of ceramization. Due to the formation of BaF_2 nano-crystals on ceramization, a significant modification occurs in the residual glass matrix together with the creation of non-bridging oxygen, which is evidenced from the FTIR study. This increase of non-bridging oxygen atoms in the residual glass matrix could be the possible reason for the red shift of the absorption edge.

The NIR absorption spectra of all Pr^{3+}-doped glass and glass ceramic samples are shown in Fig. 7 (b). It is observed that for all the samples studied here the transitions $^3H_4 \rightarrow {}^3F_3$, $^3H_6$, and $^3H_5$ occur at 1521, 2275, 3574 nm, respectively. The transition $^3H_4 \rightarrow {}^3F_2$ shows two Stark

components at 1831 nm and 1931 nm whose relative intensities change with the degree of ceramization. The component at 1931 nm is stronger for the OFPrG sample whereas the one at 1831 is dominant for ceramized OFPrGC04 and OFPrGC24 samples. Among Pr^{3+} energy level transitions, this is being a hypersensitive transition following the spectral rules of $\Delta S = 0$, $\Delta L \leq 2$ and $\Delta J \leq 2$ and reflects the local field environment around the rare earth ions. The observed change in shape of this band could be ascribed to the obvious change around the Pr^{3+} ions from oxygen to fluorine environment in glass ceramic samples.

The phenomenological Judd–Ofelt intensity parameters were calculated applying standard J-O theory[29,30]on the measured absorption spectra of precursor glass and glass ceramics samples in order to understand the changes in local structure and bonding in the vicinity of the dopant ion on ceramization. The well defined absorption peaks such as $^3H_4 \rightarrow {}^3F_2$, $^3F_3$, $^1G_4$, $^1D_2$, $^3P_0$, $^3P_1$ and $^3P_2$ have been considered for the analysis. Table IV presents the values of estimated intensity parameters. From the table it is clear that, with the increase in degree of ceramization, Ω_2 decreased significantly but the variation of Ω_4 is not so significant. For the precursor glass sample, the intensity parameters are found to be in the order $\Omega_4 < \Omega_2 < \Omega_6$, whereas, the order of the intensity parameters are $\Omega_2 < \Omega_4 < \Omega_6$ for the glass ceramics samples. This indicates a significant modification in the local structure and bonding in the vicinity of Pr^{3+} ions. Among the three J-O parameters, the dependence of Ω_2 on the local structure mainly reflects the symmetry and nature of bonding between rare earth and ligands.[31] It decreases with the increase of symmetry and with the change of nature of bond from a covalent to ionic bond. In the present study, the decrease of Ω_2 with the increase in degree of ceramization suggested that Pr^{3+} ions are incorporated into more symmetric cubic BaF_2 nano-crystals with ionic bonding nature. Similarly, the value of Ω_6 decreases with the increase of

ceramization which indicates that there is a decrease in the rigidity of the host of glass ceramics samples compared to precursor glass.

In all the samples, the observed band at 2800 nm (3571 cm^{-1}) in Fig. 7 (b) is attributed to the stretching vibration of weakly hydrogen bonded OH^- groups. The absorption coefficient α_{OH}, at 3000 cm^{-1} can be used as a measure of the OH^- concentration as suggested by Ebendorff-Heidepriem[32]:

$$\alpha_{OH} = \log\left(\frac{T_0}{T_D}\right) \times \frac{1}{d} \qquad (1)$$

where, T_o is the highest transmission, T_D is the transmission at 3000 cm^{-1} and d is the thickness of the sample. In the rare earth doped glasses, OH^- groups act as fluorescence quenching sites, which promote non-radiative decay of emitting level and ultimately decreasing the emission efficiency. The higher is the absorption coefficient; higher would be its influence on the fluorescence quenching. Hence, the measurement of hydroxyl content is very much essential. Using the expression given above, the α_{OH} is calculated to be 0.83 cm^{-1}, 1 cm^{-1}, and 1.06 cm^{-1} resulting in the estimated OH^- contents of 25, 30 and 32 ppm for OFPrG, OFPrGC04 and OFPrGC24 samples, respectively. Thus, considerably low OH^- concentrations (less than 50 ppm) for all the samples indicate that OH^- groups have a negligible effect on the fluorescence efficiency of the dopant Pr^{3+} ion in the present host systems.

(B) Excitation and emission spectra:

Fig. 8 displays the excitation spectra of Pr^{3+} ions doped glass and glass ceramic samples, by monitoring the emission at 609 nm. For OFPrG sample, there are three distinct excitation peaks from the excitation spectrum and are assigned to the transitions of Pr^{3+} like $^3H_4 \rightarrow {}^3P_2$

(444 nm), $^3H_4 \rightarrow {}^3P_1$ (467 nm) and $^3H_4 \rightarrow {}^3P_0$ (482 nm) based on the literature.[17,33,34] A weak excitation transition $^3H_4 \rightarrow {}^1I_6$ has been observed at 459 nm which is found to be more distinctive in case of glass ceramic samples similar to the observation made from absorption spectra as described in the previous section. With an increase in degree of ceramization, there is a gradual increase in excitation peak intensities. From these spectra, intense peak at (444 nm) corresponding to the energy level of $^3P_2$ has been selected for the measurement of emission spectrum.

The room temperature emission spectra of Pr^{3+} ions for the glass and glass ceramic samples in the range of 475–800 nm with an excitation at 444 nm of $^3P_2$ level are shown in Fig. 9. Among the nine measured emission peaks for OFPrG sample, six emissions are originating from $^3P_0$, two from $^3P_1$, and one from $^1D_2$ excited states. However, transition from $^1D_2$ excited state is overlapped with the transition from $^3P_0$. The emission peaks are assigned to $^3P_0 \rightarrow {}^3H_4$, $^3P_1 \rightarrow {}^3H_5$, $^3P_0 \rightarrow {}^3H_5$, $^3P_1 \rightarrow {}^3H_6$, ($^1D_2 \rightarrow {}^3H_4$, $^3P_0 \rightarrow {}^3H_6$), $^3P_0 \rightarrow {}^3F_2$, $^1D_2 \rightarrow {}^3H_5$, $^3P_0 \rightarrow {}^3F_3$, and $^3P_0 \rightarrow {}^3F_4$ transitions with the increasing order of wavelength at 484 nm, 526 nm, 544 nm, 559 nm, 610 nm, 643 nm, 681 nm, 703 nm, and 724 nm, respectively. In case of glass ceramic samples (OFPrGC04 and OFPrGC24), the emission transitions $^1D_2 \rightarrow {}^3H_4$, $^3P_0 \rightarrow {}^3H_6$ are well resolved and the intensity of each transition is enhanced significantly. From the spectra it is also observed that, in OFPrG sample, the red emission at 607 nm ($^1D_2 \rightarrow {}^3H_4$, $^3P_0 \rightarrow {}^3H_6$) is more intense over all other recorded emission peaks which is normally observed in many other hosts. But in OFPrGC4 and OFPrGC24 samples, the blue emission peak at 484 nm has remarkably increased its intensity by three folds over the red emission peak. These variations of fluorescence intensity of individual peaks and their relative intensity ratio as a function of ceramization condition are graphically represented in the inset of Fig.9. The relative intensity ratio of $^3P_0 \rightarrow {}^3H_4$ (blue) to [$^1D_2 \rightarrow {}^3H_4$, $^3P_0 \rightarrow {}^3H_6$] (red) for OFPrG,

OFPrGC04 and OFPrGC24 samples are 0.91, 2.30 and 2.36, respectively. The increase in the intensity of blue peak in ceramized samples could be explained on the basis of the energy level structure of Pr^{3+} ions and the lattice phonon energy as follows: the energy gap between $^3P_0$ and $^1D_2$ is found to be 4042 cm^{-1} (inset of Fig. 10) and the highest phonon energy available in the present glassy host is around 1100 cm^{-1} (from FTIR). Hence only four phonons are sufficient enough to bridge the gap between $^3P_0$ and $^1D_2$ energy states. But while the dopant ion enters into crystalline phase (BaF_2) having phonon energy of 346 cm^{-1},[16] it requires around 12 phonons to fill this energy gap. It is well known that, when the required number of phonons is more than 5, the phonon assisted non-radiative relaxation does not occur.[35] So, in the present situation, the enhanced blue emission with the increase in ceramization could be attributed to the increased radiative transition from $^3P_0$ to ground state as a consequence of substantial decrease in non-radiative relaxation of $^3P_0$ to $^1D_2$ state. Thus, the relative intensity of [$^3P_0 \rightarrow {}^3H_4$] and [$^1D_2 \rightarrow {}^3H_4$, $^3P_0 \rightarrow {}^3H_6$] increases with the increase in degree of ceramization for OFPrGC04 and OFPrGC24 samples. It is observed that the intensity of the emission transitions $^3P_0 \rightarrow {}^3H_4$ (blue) and [$^1D_2 \rightarrow {}^3H_4$, $^3P_0 \rightarrow {}^3H_6$] (red) is almost equal in tellurite glasses[17] (phonon energy = 677 cm^{-1}) whereas the blue emission dominates many folds compared to red emission transition in BaF_2 single crystalline hosts[18,19] (phonon energy = 346 cm^{-1}). However, in oxide hosts (phonon energy $\geq$ 1100 cm^{-1}), Pr^{3+} exhibits dominant red emission in general.[36] In the present study, it has been found from the measured fluorescence spectral features that, in the precursor glass, red emission dominates over blue similar to oxide systems. But, in heat-treated glass-ceramics, blue emission dominates over red like in fluoride crystal. The reason for this phenomenon is attributed to the restricted non-radiative relaxation from $^3P_0$ to $^1D_2$ level in low phonon hosts as described above.

In order to further investigate and confirm the effect of co-existence of contributions from $^3P_0$ and $^1D_2$ levels in the red emission at 575–635 nm transition in detail, the time resolved emission spectra analysis has been carried out for OFPrG sample by an excitation at 444 nm ($^3H_4 \rightarrow {}^3P_2$) with various delay times as shown in Fig. 10. The peaks are well resolved for delay times of 0.02 ms and 0.05 ms due to the differences in the lifetimes of the two excited states $^3P_0$ and $^1D_2$. The intensity of the peak with time delay of 0.1 ms becomes considerably quenched due to significant decay for both $^1D_2 \rightarrow {}^3H_4$ and $^3P_0 \rightarrow {}^3H_6$ transitions. It can be observed from this figure that, with an increase in the time delay from 0.01 ms to 0.1 ms, the intensity of the transition $^3P_0 \rightarrow {}^3H_6$ decreases more rapidly than the transition emission from $^1D_2 \rightarrow {}^3H_4$. Furthermore, the measured decay curves of emission bands as shown in Fig. 11 (a) and (b) show that $^3P_0$ level decays faster than $^1D_2$ for all the samples. The lifetimes estimated from the recorded decay curves for the $^1D_2 \rightarrow {}^3H_4$ transition by exciting at 444 nm are 51, 75, and 78 μs for the OFPrG, OFPrGC04 and OFPrGC24 samples, respectively, whereas the lifetimes calculated for the $^3P_0 \rightarrow {}^3H_6$ transition under same excitation are 40, 53, and 54 μs for the OFPrG, OFPrGC04 and OFPrGC24 samples, respectively. On ceramization, the lifetime increases slightly for both $^1D_2 \rightarrow {}^3H_4$ and $^3P_0 \rightarrow {}^3H_6$ transitions.

II. Conclusions

The transparent glass ceramics containing Pr^{3+}:BaF_2 nano-crystallites have been successfully prepared and systematically analyzed for thermal, structural and luminescence properties through DTA, XRD, TEM, FTIRRS, absorption and fluorescence spectral measurements. XRD and TEM investigation confirmed the presence of face centred cubic BaF_2 nano-crystals dispersed in the glass matrix of heat treated samples with an average crystallite size in the

range of 7.7 – 7.9 nm. Thorough study of XRD patterns by Rietveld analysis also resulted in the estimation of wt% of crystalline and residual amorphous phases, microstrain parameters. The recorded optical absorption and fluorescence spectra exhibited non-degenerated peaks for certain transitions which are otherwise degenerated in precursor glass demonstrating that the dopant ion has entered in the BaF_2 crystalline phase. For the first time, from the observed changes in the shape of absorption peak of transition $^3H_4 \rightarrow {}^3P_0$ of Pr^{3+}, the local field environment of dopant ions could be realized in glass and glass ceramic samples. By applying standard Judd-Ofelt theory on the well defined absorption peaks from measured UV-Vis-NIR absorption spectra, three phenomenological intensity parameters (Ω_2, Ω_4 and Ω_6) have been computed by least square fitting method. The decrease in the value of Ω_2 for the ceramized samples compared to precursor glass has been observed which was ascribed to the incorporation of Pr^{3+} into the BaF_2 nano-crystals. A remarkable increase (by 3 fold) of relative intensity ratio of blue ($^3P_0 \rightarrow {}^3H_4$) to red ($^1D_2 \rightarrow {}^3H_4$, $^3P_0 \rightarrow {}^3H_6$) emissions is observed for glass ceramics samples compared to glass which was ascribed due to drastic decrease of multiphonon non-radiative relaxation from $^3P_0$ to $^1D_2$ level. Time resolved spectra exhibit $^3P_0$ level decays faster than $^1D_2$ level.

Acknowledgements

Authors would like to express their grateful thanks to Dr. H. S. Maiti, Director, CGCRI for his kind cooperation and encouragement in the publication of this manuscript. We are also thankful to Dr. Ranjan Sen, Scientist In-Charge, for his continued support. One of us (ADS) expresses profound thanks to the CGCRI, CSIR for the award of a Research Internship to him.

References

[1]W. Length, and R.M. McFarlane, "Upconversion Lasers," *Opt. Photonics News,* **3**, 8-15 (1992).

[2]A.J. Kenyon, "Recent Developments in Rare-Earth Doped Materials for Optoelectronics," *Prog. Quantum Electron.,* **26**, 225–84 (2002).

[3]M. Mortier, P. Goldner, C. Chateau, and M. Genotelle, "Erbium Doped Glass–Ceramics: Concentration Effect on Crystal Structure and Energy Transfer between Active Ions," *J. Alloys Comp*., **323-324,** 245-49 (2001).

[4]Y. Wang, and J. Ohwaki, "New Transparent Vitroceramics Codoped With Er^{3+} and Yb^{3+} For Efficient Frequency Upconversion," *Appl. Phys. Lett.,* **63,** 3268-70 (1993).

[5]M. J. Dejneka, "Transparent Oxyfluoride Glass Ceramics," *MRS Bull.,* **23**, 57-62 (1998).

[6]M. J. Dejneka, "The Luminescence and Structure of Novel Transparent Oxyfluoride Glass – Ceramics," *J. Non-Cryst. Solids*, **239,** 149-55 (1998).

[7]M. Mattarelli, V. K. Tikhomirov, A. B. Seddon, M. Montagna, E. Moser, A. Chiasera, S. Chaussedent, G. Nunzi Conti, S. Pelli, G.C. Righini, L. Zampedri, and M. Ferrari, "Tm^{3+}-Activated Transparent Oxy-Fluoride Glass–Ceramics: Structural And Spectroscopic Properties," *J. Non-Cryst. Solids*, **345-346**, 354-58 (2004).

[8]P. Nachimuthu, Muga Vithal, and R. Jagannathan, "Judd-Ofelt Parameters, Hypersensitivity, and Emission Characteristics of Ln^{3+} ($Nd^{3+,}$ $Ho^{3+,}$ and Er^{3+}) Ions Doped in PbO-PbF_2 Glasses," *J. Am. Ceram. Soc*., **82**, 387-92 (1999).

[9]S. Fujihara, T. Kato, and T. Kimura, "Sol–Gel Synthesis of Silica-Based Oxyfluoride Glass-Ceramic Thin Films: Incorporation of Eu^{3+} Activators into Crystallites," *J. Am. Ceram. Soc.,* **84,** 2716–18 (2001).

[10]S. Tanabe, H. Hayashi, and T. Hanada, "Improved Fluorescence from Tm-Ho- and Tm-Ho-Eu-Codoped Transparent PbF_2 Glass-Ceramics for S^+-Band Amplifiers," *J. Am. Ceram. Soc.,* **85,** 839–43 (2002).

[11]S. Tanabe, H. Hayashi, and T. Hanada, "Improved Fluorescence from Tm-Ho- and Tm-Ho-Eu-Codoped Transparent PbF_2 Glass-Ceramics for S^+-Band Amplifiers," *J. Am. Ceram. Soc.,* **85,** 839–43 (2002).

[12]P. Nachimuthu, Muga Vithal, and R. Jagannathan, "Absorption and Emission Spectral Properties of Pr^{3+}, Nd^{3+}, and Eu^{3+} Ions in Heavy-Metal Oxide Glasses," *J. Am. Ceram. Soc*., **83,** 597–604 (2000).

[13]C. Yu, J. Zhang, and Z. Jiang, "Influence of Heat Treatment on Spectroscopic Properties of Er^{3+} in Multicomponent ZrF_4–ZnF_2–AlF_3–YF_3–MF_2 (M = Ca, Sr, Ba) Based Glass," *J. Non-Cryst. Solids*, **353**, 2654-58 (2004).

[14]V. Grover, S. N. Achary, S. J. Patwe, and A. K. Tyagi, "Synthesis and Characterization of $Ba_{1-x}Nd_xF_{2+x}$ ($0.00 \leq X \leq 1.00$)," *MRS Bull.,* **38,** 1101-11 (2003).

[15]Y. Yu, D. Chen, Y.Wang , F. Liu, and E. Ma, "A new transparent oxyfluoride glass ceramic with improved luminescence," *J. Non-Cryst. Solids,* **353,** 405–09 (2007).

[16]X. Qiao, X. Fan, and M. Wang, "Luminescence behavior of Er^{3+} in glass ceramics containing BaF_2 nanocrystals," *Script. Mater*. **55,** 211–14 (2006).

[17]K. Annapurna , R. Chakrabarti, and S. Buddhudu, "Absorption and emission spectral analysis of Pr^{3+}: tellurite glasses," *J. Mater. Sci*., **42**, 6755-61 (2007).

[18]P. A. Rodnyi, G. B. Stryganyuk, C. W. E. van Eijk, and A. S. Voloshinovskii, "Variation of 5*d* -level position and emission properties of BaF_2:Pr crystals," *Phys. Rev. B*, **72**, 195112pp. (2005).

[19]H. Sato, "Preparation of praseodymium-doped single crystal barium fluoride thin film on CaF_2 by chemical vapour," *Jap. J. Appl. Phys.,* **33,** L371-L373 (1994).

[20]H. M. Rietveld, "A profile refinement method for nuclear and magnetic structures," *J. Appl. Cryst.*, **2**, 65-71 (1969).

[21]R. A. Young, "Introduction to the Rietveld method"; pp. 1-39 in *The Rietveld Method*, Edited by R. A. Young, Oxford University Press, Oxford, 1993.

[22]www. PANalytical.com

[23]

[24]C. Bocker, and C. Rüssel, "Self-organized nano-crystallisation of BaF_2 from $Na_2O/K_2O/BaF_2/Al_2O_3/SiO_2$ glasses," *J. Eur. Ceram. Soc.,* **29**, 1221-25 (2009).

[25]C. I. Merzbacher, and W.B. White, "The structure of alkaline earth aluminosilicate glasses as determined by vibrational spectroscopy*," J. Non-Cryst. Solids,* **130,** 18-34 (1991).

[26]D. S. Wang, and C. G. Pantano, "Structural characterization of $CaO-B_2O_3-Al_2O_3-SiO_2$ xerogels and glasses," *J. Non-Cryst. Solids,* **142,** 225-33 (1992).

[27] M. Toderas, S. Filip, and I. Ardelean, "Structural study of the $Fe_2O_3-B_2O_3$-BaO glass system by FTIR spectroscopy," *J. Optoelectron. Adv. Mater.*, **8,** 1121-3 (2006).

[28]K. Binnemans, and C. Görller-Walrand, "On the color of the trivalent lanthanide ions," *Chem. Phys. Lett.,* **235**, 163-74 (1995).

[29]B. R. Judd, "Optical absorption intensities of rare-earth ions," *Phys. Rev.* **127**, 750-61 (1962).

[30] G. S. Ofelt, "Intensities of crystal spectra of rare-earth ions," *J. Chem. Phys.* **37,** 511-20 (1962).

[31]S. Tanabe, T. Ohyagi, N. Soga, and T. Hanada, "Compositional dependence of Judd-Ofelt parameters of Er^{3+} ions in alkali-metal borate glasses," *Phys. Rev. B*, **46,** 3305-10 (1992).

[32]H. Ebendorff-Heidepriem, W. Seeber, and D. Ehrt, "Dehydration of phosphate glasses," *J. Non Cryst. Solids,* **163**, 74-80 (1993).

[33]A. Remillieux, B. Jacquier, C. Linares, C. Lesergent, S. Artigaud, D. Bayard, L. Hamon, J.L. Beylat, "Upconversion mechanisms of a praseodymium-doped fluoride fibre amplifier," *J. Phys. D: Appl. Phys,.* **29**, 963-74 (1996).

[34]G. Jose, V. Thomas, G. Jose, P. I. Paulose, and N. V. Unnikrishnan, "Application of a modified Judd-Ofelt theory to Pr^{3+} doped phosphate glasses and the evaluation of radiative properties," *J. Non-Cryst. Solids,* **319,** 89-94 (2003).

[35]M. D. Shinn, W. A. Sibley, M. G. Drexhage, and R. N. Brown, "Optical transitions of Er^{3+} ions in fluorozirconate glasses," *Phys. Rev. B*. **27,** 6635–48 (1983).

[36]X. Zhang, J. Zhang, X. Ren, and X. J. Wang, "The dependence of persistent phosphorescence on annealing temperatures in $CaTiO_3:Pr^{3+}$ nanoparticles prepared by a coprecipitation technique," *J. Solid State Chem.*, **181,** 393-98 (2008).

Figure Captions

Fig. 1. Photograph of the (a) as-prepared glass (OFPrG) and glass ceramic samples ceramized at 600^{o}C for (b) 4 h (OFPrGC04), and (c) 24 h (OFPrGC24).

Fig. 2. Differential thermal analysis (DTA) curve of as-prepared glass powder.

Fig. 3. XRD patterns of glass and glass ceramic samples.

Fig. 4. X-ray diffraction patterns of the OFPrGC24 sample along with difference plot as obtained by Rietveld refinement.

Fig. 5. (a) TEM bright field image, and (b) Selected area electron diffraction (SAED) pattern for OFPrGC04 sample.

Fig. 6. FTIR reflectance spectra of glass and glass ceramic samples.

Fig. 7. (a) Visible and (b) NIR absorption spectra of (a) OFPrG, (b) OFPrGC04, and (c) OFPrGC24 samples.

Fig. 8.Excitation spectra of (a) OFPrG, (b) OFPrGC04, and (c) OFPrGC24 samples with λ_{em} = 609 nm.

Fig. 9. Emission spectra of (a) OFPrG, (b) OFPrGC04, and (c) OFPrGC24 samples with λ_{ex} = 444 nm. (Inset) The intensity of blue and red emission and the relative intensity of blue to red emission are plotted against ceramization time.

Fig. 10. Time resolved emission spectra of glass and glass ceramic samples with λ_{ex} = 444 nm at different delay times of (a) 0.01, (b) 0.02, (c) 0.05, and (d) 0.10 ms. (inset: simplified energy level diagram of Pr^{3+} in the present host)

Fig. 11. Fluorescence decay curves of (a) $^{1}D_{2}$ and (b) $^{3}P_{0}$ levels of all the glass and glass ceramic samples with λ_{ex} = 444 nm.

Table I. Different physical, optical properties of precursor glass (OFPrG) and glass ceramic samples (OFPrGC04 and OFPrGC24).

Properties		**Samples**		
		OFPrG	OFPrGC04	OFPrGC24
Average molecular weight		99.3	99.3	99.3
Density, g cm^{-3}		3.21	3.19	3.19
Refractive Indices	**473 nm**	1.5574	1.5534	1.5527
	532 nm	1.5525	1.5488	1.5483
	632.8 nm	1.5476	1.5445	1.5436
	1064 nm	1.5386	1.5346	1.5340
	1552 nm	1.5333	1.5300	1.5295
Mean dispersion $(n_{F'}-n_{C'})$		0.0094	0.0088	0.0088
Abbe number $(n_E-1)/(n_{F'}-n_{C'})$		58.7	62.3	62.3
Reflection loss, R%		4.681	4.634	4.624
Molar refractivity, R_M, cm^3		9.887	9.896	9.885
Molecular electronic polarizability, α_e, cm^3 ($\times 10^{-24}$)		3.921	3.925	3.920
Rare earth concentration, N, (ions/cm^3) ($\times 10^{21}$)		9.735	9.674	9.674
Ionic radius, r_p, Å		1.920	1.924	1.924
Inter-ionic distance, r_i, Å		5.544	5.556	5.556
Field Strength, F, cm^2($\times 10^{15}$)		8.142	8.108	8.108

Table II. Estimated values of Wt.% of crystalline and amorphous phases, size, strain and lattice parameters of crystalline BaF_2 of the glass ceramic samples from Rietveld analysis

Sample	**wt. % Phases**		**crystalline BaF_2**		**Lattice parameters (nm)**
	Amorphous	**Crystalline**	**Size (Å)**	**Strain (%)**	
OFPrGC04	88.79	11.21	78.6	0.072	a = b = c = 0.617
OFPrGC24	87.74	12.26	77.0	0.068	a = b = c = 0.617

Size---Average crystallite size (Å), **Strain**------Average Microstrain (%)

Table III. Evaluated reliability parameters of the glass ceramic samples from the Rietveld analysis

Sample	R_{exp}	R_p	R_{wp}	D_{ws}	GOF
OFPrGC04	9.18265	9.01105	11.13036	0.81814	1.46921
OFPrGC24	9.14417	9.06341	11.31891	0.72453	1.53222

Table IV. Calculated Judd-Ofelt intensity parameters $\Omega_{\lambda,}$ where λ=2, 4, 6 of Pr^{3+} doped glass and glass ceramics samples.

Sample	Ω_2 ($\times 10^{20}$) (cm^2)	Ω_4($\times 10^{20}$) (cm^2)	Ω_6 ($\times 10^{20}$) (cm^2)
OFPrG	2.65526	1.43506	3.26386
OFPrGC04	0.44429	1.1995	2.2636
OFPrGC24	0.34969	1.16389	2.24914

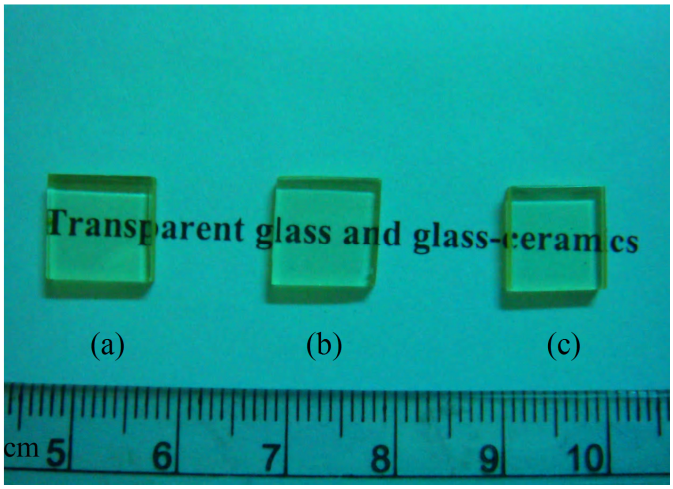

Fig. 1

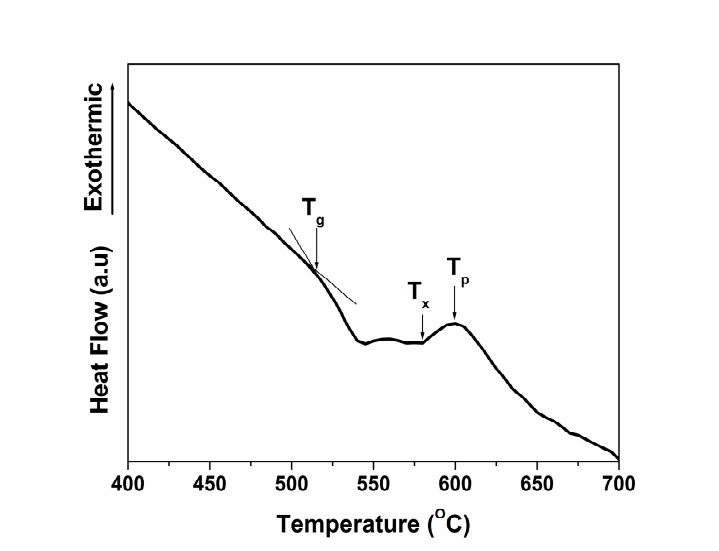
Exothermic
Heat Flow (a.u)
T_g
T_x
T_p
400
450
500
550
600
650
700
Temperature (°C)

Fig. 2

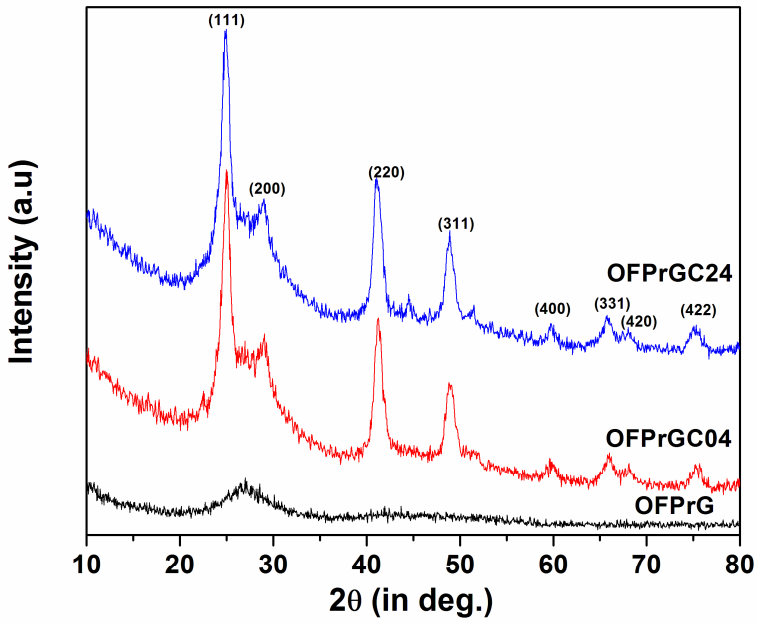
(111)
(200)
(220)
(311)
(400)
(331)
(420)
(422)
OFPrGC24
OFPrGC04
OFPrG
Intensity (a.u)
10
20
30
40
50
60
70
80
2θ (in deg.)

Fig. 3

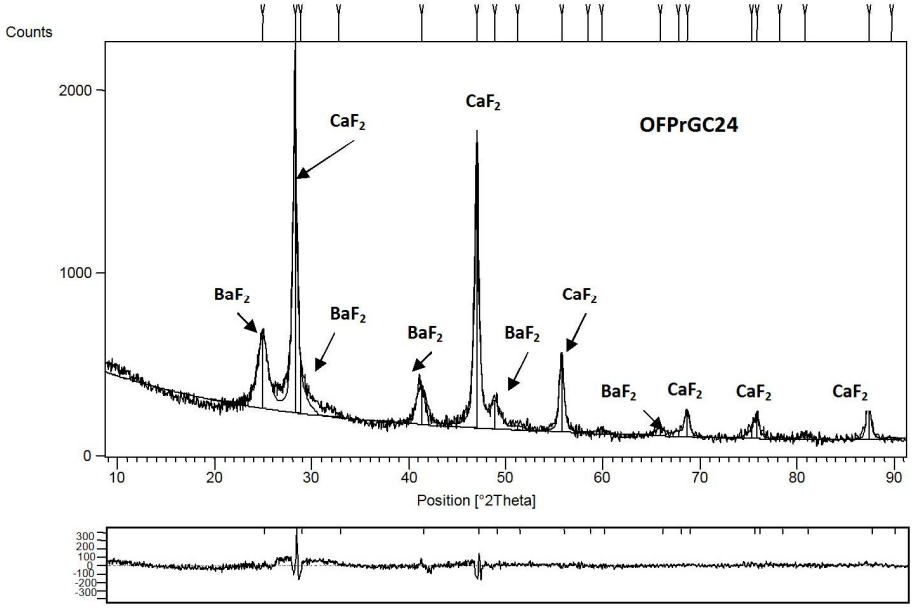
Counts
2000
1000
0
CaF2
CaF2
OFPrGC24
BaF2
BaF2
BaF2
BaF2
CaF2
BaF2
CaF2
CaF2
CaF2
10
20
30
40
50
60
70
80
90
Position [°2Theta]
300
200
100
0
-100
-200
-300

Fig. 4

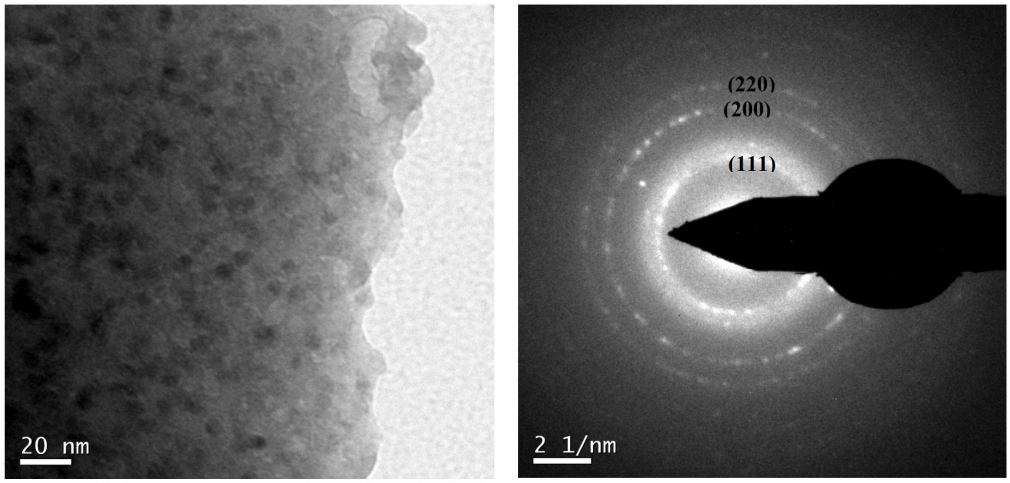

(a) (b)

Fig. 5

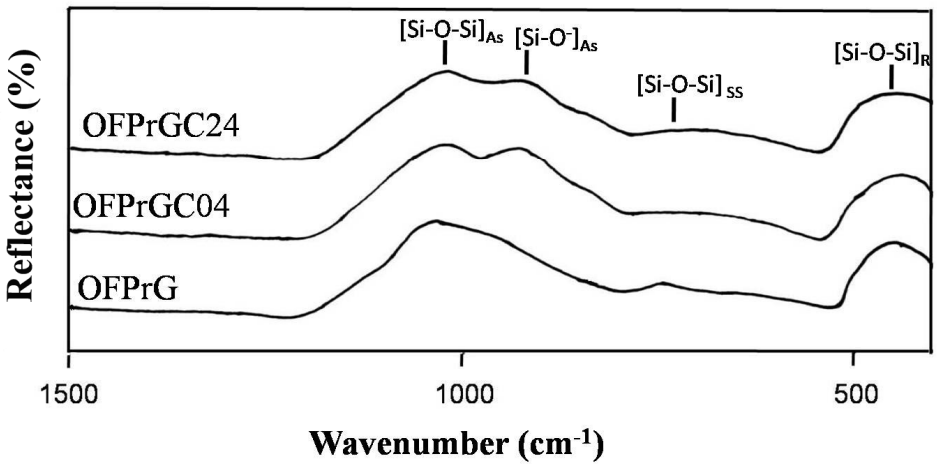
[Si-O-Si]As
[Si-O-]As
[Si-O-Si] SS
[Si-O-Si]R
OFPrGC24
OFPrGC04
OFPrG
Reflectance (%)
1500
1000
500
Wavenumber (cm-1)

Fig. 6

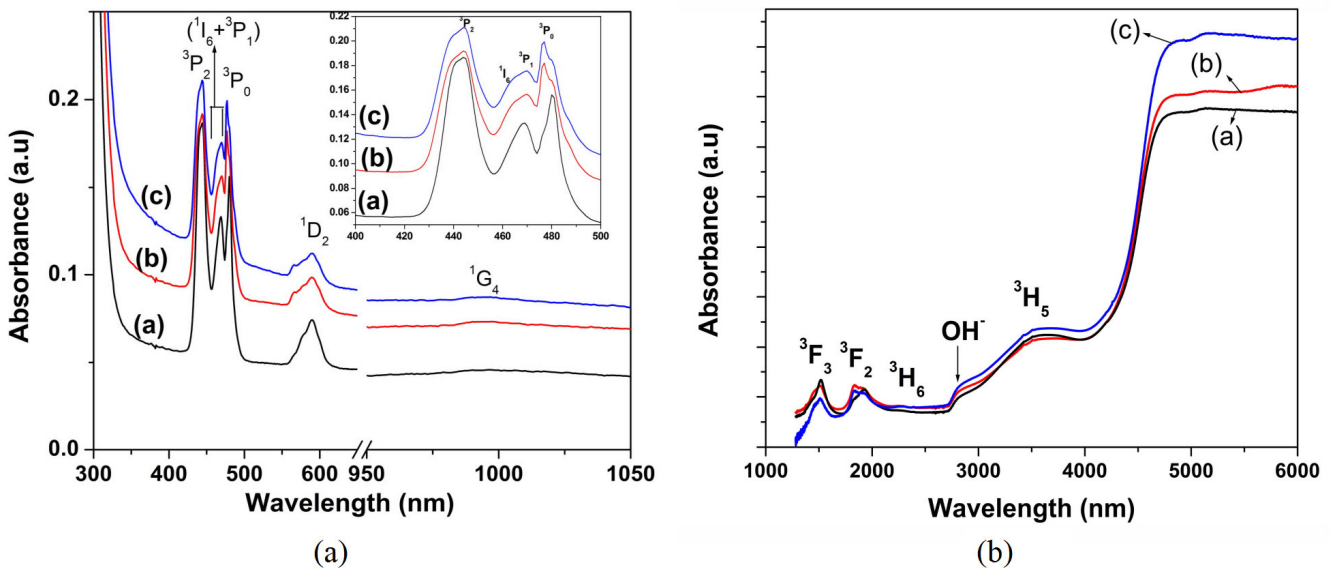
Absorbance (a.u)
Wavelength (nm)
(c)
(b)
(a)
$(^1I_6+^3P_1)$
$^3P_2$
$^3P_0$
$^1D_2$
$^1G_4$
$^3F_3$
$^3F_2$
$^3H_6$
OH^-
$^3H_5$

(a) (b)

Fig. 7

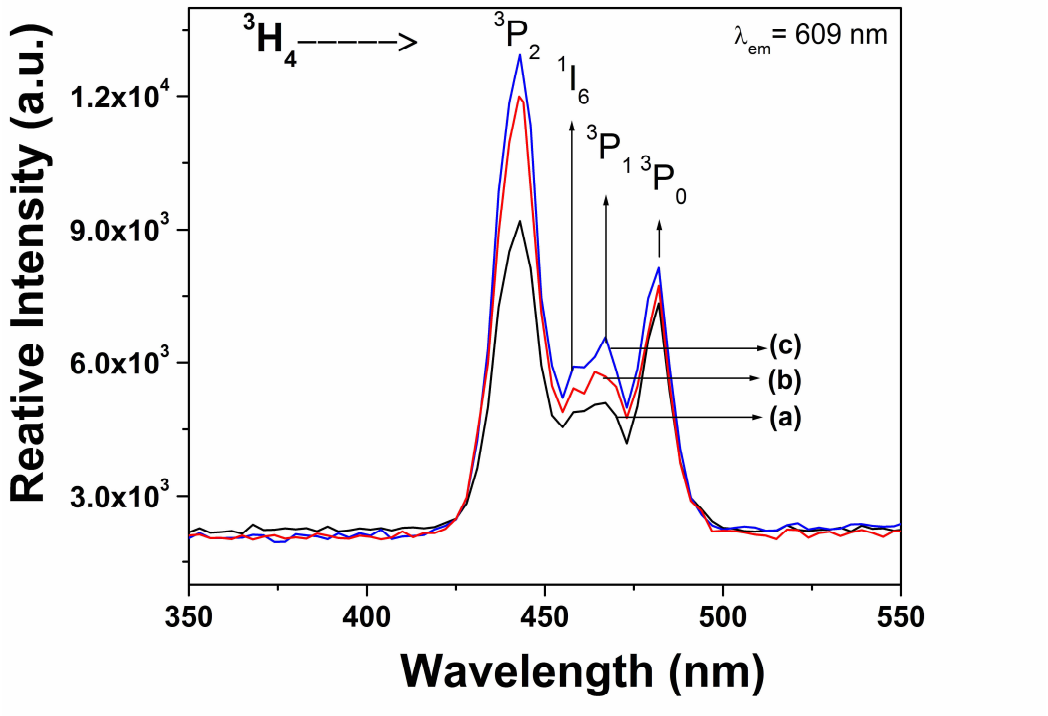
$^3H_4$------>
$^3P_2$
$^1I_6$
$^3P_1$
$^3P_0$
λ_{em}= 609 nm
(c)
(b)
(a)
Reative Intensity (a.u.)
1.2x10^4
9.0x10^3
6.0x10^3
3.0x10^3
350
400
450
500
550
Wavelength (nm)

Fig. 8

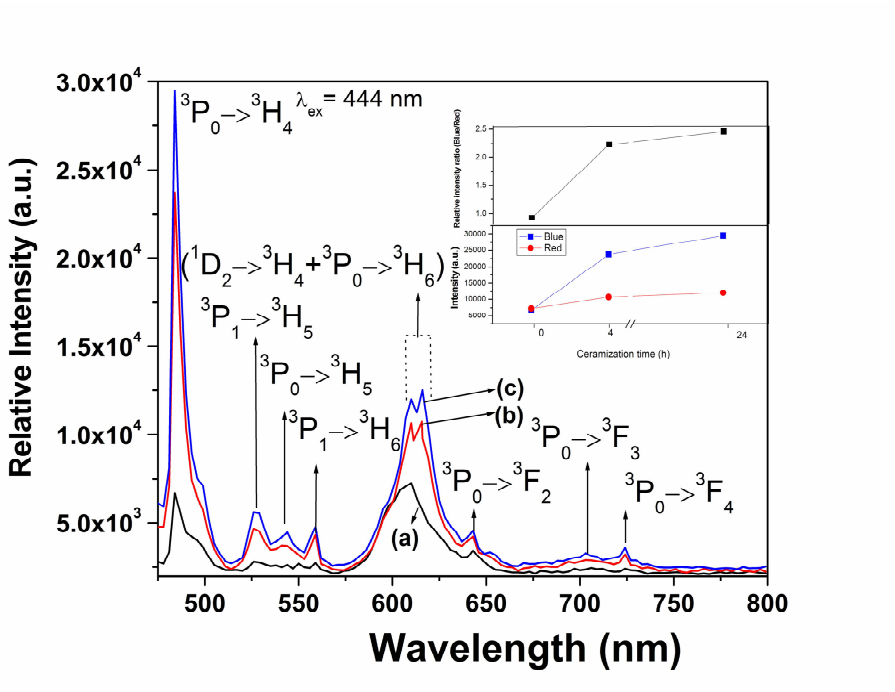
3.0x10^4
2.5x10^4
2.0x10^4
1.5x10^4
1.0x10^4
5.0x10^3
Relative Intensity (a.u.)
500
550
600
650
700
750
800
Wavelength (nm)
3P0->3H4 λex= 444 nm
(1D2->3H4+3P0->3H6)
3P1->3H5
3P0->3H5
3P1->3H6
(c)
(b)
(a)
3P0->3F3
3P0->3F2
3P0->3F4
Blue
Red
Ceramization time (h)

Fig. 9

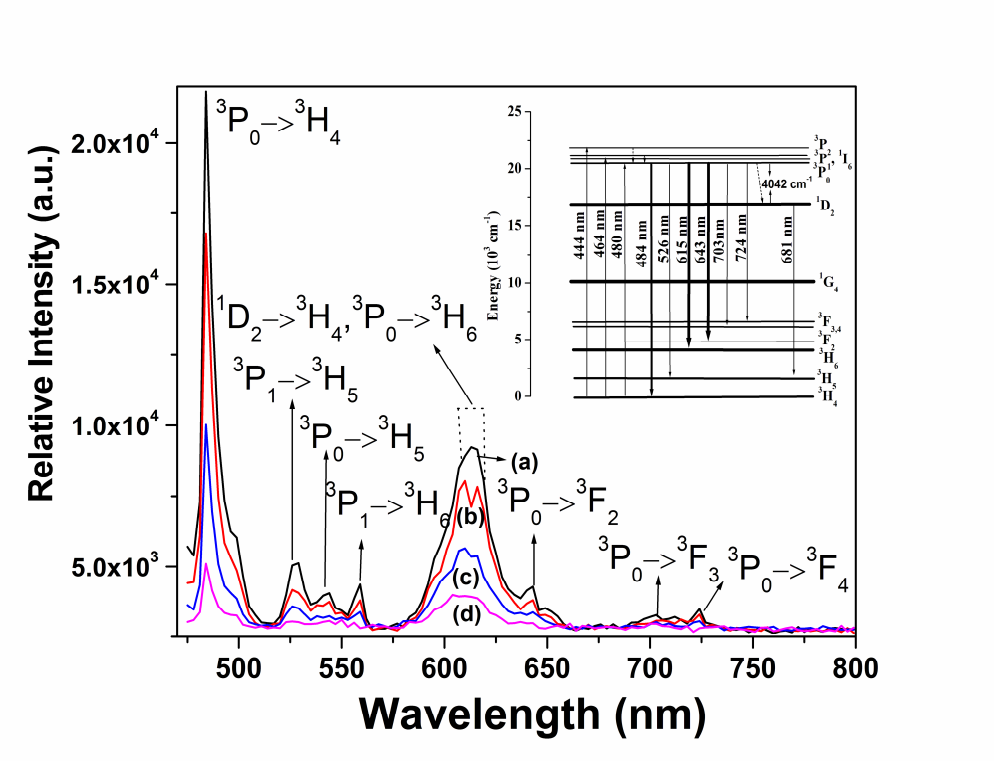
Relative Intensity (a.u.)
2.0x10^4
1.5x10^4
1.0x10^4
5.0x10^3
500
550
600
650
700
750
800
Wavelength (nm)
3P0->3H4
1D2->3H4, 3P0->3H6
3P1->3H5
3P0->3H5
3P1->3H6
3P0->3F2
3P0->3F3
3P0->3F4
(a)
(b)
(c)
(d)
Energy (10^3 cm^-1)
4042 cm^-1
444 nm
464 nm
480 nm
484 nm
526 nm
615 nm
643 nm
703nm
724 nm
681 nm
1D2
1G4
3F3,4
3F2
3H6
3H5
3H4

Fig. 10

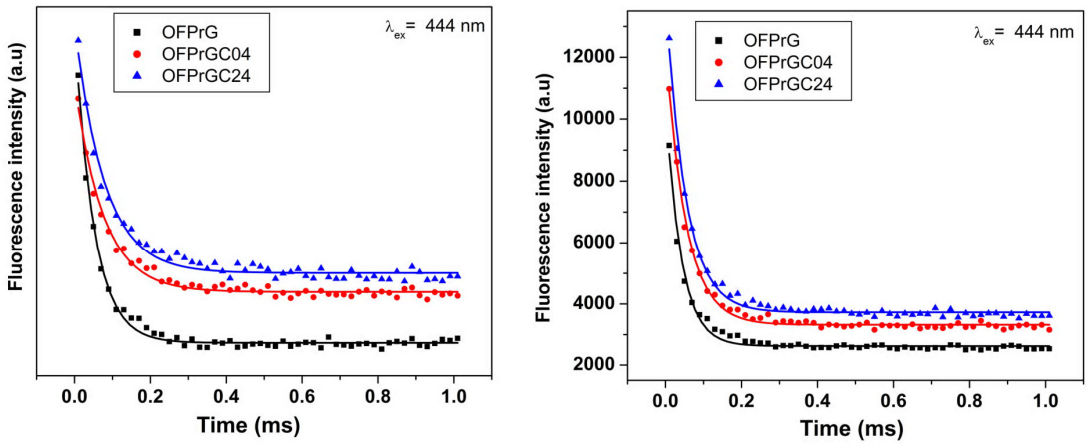
OFPrG
OFPrGC04
OFPrGC24
λex = 444 nm
Fluorescence intensity (a.u)
Time (ms)
0.0
0.2
0.4
0.6
0.8
1.0
2000
4000
6000
8000
10000
12000
(a)
(b)

Fig. 11